

Dehydrogenation of Cyclohexanol on Fe, Ti-MCM-41 Mesoporous Materials

M. Popova · Á. Szegedi · K. Lázár ·
A. Dimitrova

Received: 17 March 2011 / Accepted: 16 June 2011 / Published online: 6 July 2011
© Springer Science+Business Media, LLC 2011

Abstract Iron and titanium modified MCM-41 materials, prepared by direct synthesis were investigated using X-ray diffraction (XRD), nitrogen physisorption, UV–Vis diffuse reflectance, Mössbauer, FT-IR and EPR spectroscopies. Materials with high surface area and well-ordered pore structure were obtained. All modified mesoporous silicas possess high activity in cyclohexanol conversion. FeTiMCM-41 ($\text{Si}/\text{Ti} = 10$, $\text{Si} + \text{Ti}/\text{Fe} = 15$) catalyst presented the highest activity and selectivity to cyclohexanone.

Keywords Cyclohexanol dehydrogenation · FeTiMCM-41

1 Introduction

MCM-41 silica materials, with their uniform mesoporous channel structure and high specific surface area are of particular interest as catalyst support [1–8]. A wide variety

of metal ions (Fe, Ti, V, Cr, Cu, etc.) has been introduced into the silica matrix to obtain materials with tunable catalytic properties [9–11]. It has been established, that the applied method of modification strongly influences the state (localization, dispersion and oxidative state) of the loaded metal species [12–15]. Their introduction in the host matrix could be realized during the silica synthesis procedure as well as by various postsynthesis techniques (impregnation, grafting) [12–16]. However, the preparation of stable, modified materials by conventional hydrothermal synthesis is usually possible at low metal loading, which strongly restricts the application as catalysts. It has been recently reported that the sol–gel technique reveals much higher ability in this aspect, and the preparation of stable metal modified MCM-41 materials were obtained [12, 13, 17].

Dehydrogenation of cyclohexanol to cyclohexanone is a very important industrial process because cyclohexanone is an intermediate used in the production of caprolactam. Both surface acid–base characteristics and redox properties of the catalysts influence dehydrogenation of cyclohexanol. Investigations have focused on the influence of the support, the method of preparation, and the metal loading on the activity and selectivity of the catalysts in order to enhance the alcohol conversion [18–31]. Incorporation of iron can modify the acidity and redox properties of the host structure. The catalytic behavior of copper–iron binary oxides in the dehydrogenation of cyclohexanol has been studied by Chen et al. [32]. The yield of cyclohexanone reached 79% on $\text{Cu}-\text{Fe}_3\text{O}_4$, much higher than that on $\text{Cu}-\text{ZnO}$ (ca. 56%), which is the conventional catalyst for this reaction. Dehydrogenation of cyclohexanol to cyclohexanone has been also studied on various Group VIII metals catalysts (Fe, Co, Re, Ru) and they show high selectivity to cyclohexanone [33]. In our previous investigations the

M. Popova (✉)
Institute of Organic Chemistry with Centre of Phytochemistry,
Bulgarian Academy of Sciences, Acad. G. Bonchev str., bl.9,
1113 Sofia, Bulgaria
e-mail: mpopova@orgchm.bas.bg

Á. Szegedi
Institute of Nanochemistry and Catalysis, Chemical Research
Center, Hungarian Academy of Sciences, Pusztaszéri út 59-67,
Budapest 1025, Hungary

K. Lázár
Institute of Isotopes, Hungarian Academy of Sciences,
PO Box 77, Budapest 1525, Hungary

A. Dimitrova
Institute of Catalysis, Bulgarian Academy of Sciences,
1113 Sofia, Bulgaria

stabilization effect of titanium on the iron species incorporated into the MCM-41 matrix, being important active sites in toluene oxidation, was investigated [34]. To the best of our knowledge no data are available for the application of iron and titanium modified MCM-41 materials as a catalyst for cyclohexanol dehydrogenation.

In the present study, we focus on the catalytic behavior of iron and titanium modified mesoporous MCM-41 in cyclohexanol dehydrogenation.

2 Experimental

2.1 Synthesis

Silica MCM-41, the monocomponent TiMCM-41 and FeMCM-41 materials and the bicomponent titanium- and iron containing samples (TiFeMCM-41) were prepared at room temperature by the procedure described in our previous papers [34, 35]. Tetraethyl orthosilicate (TEOS, Aldrich) and tetraethyl orthotitanate (Ti(OEt)_4 , Aldrich) were used as silica and titania sources, respectively. Typically, 10.4 mL of TEOS was mixed with 1 mL of Ti(OEt)_4 in 10.4 mL propan-2-ol, and 0.9 g of $\text{Fe(NO}_3)_3 \cdot 9\text{H}_2\text{O}$. The clear solution was cooled down to 283 K and poured directly to the solution containing 2.5 g *N*-hexadecyltrimethylammonium bromide ($\text{C}_{16}\text{TMABr}$) and 10 mL of conc. ammonia solution (25 wt%) in 125 mL water. The precipitated suspensions were stirred for 2 h and aged overnight at room temperature. Because of its ammonia content the pH of the synthesis mixture was highly alkaline (about 12) and the synthesis products were washed with distilled water until neutral pH was reached. After drying at 333 K, the template removal was carried out at 813 K in air with a heating rate of 1 K/min. Prepared bicomponent materials were designated as $\text{FeTiMCM-41}(x)$, where $x = 1$ for FeTiMCM-41 ($\text{Si/Ti} = 10$, $\text{Si + Ti/Fe} = 15$); $x = 2$ for FeTiMCM-41 ($\text{Si/Ti} = 10$, $\text{Si + Ti/Fe} = 25$); $x = 3$ for FeTiMCM-41 ($\text{Si/Ti} = 20$, $\text{Si + Ti/Fe} = 15$); $x = 4$ for FeTiMCM-41 ($\text{Si/Ti} = 20$, $\text{Si + Ti/Fe} = 25$). The mono-component modifications were designated as TiMCM-41 and FeMCM-41.

2.2 Characterization

X-ray diffractograms were recorded by Philips PW 1810/1870 diffractometer applying monochromatized $\text{Cu K}\alpha$ radiation (40 kV, 35 mA).

Nitrogen physisorption measurements were carried out at 77 K using Quantachrome NOVA Automated Gas Sorption Instrument. The pore-size distributions were calculated from the desorption isotherms with the BJH method.

Diffuse reflectance spectra of the samples in the UV–Vis region were registered using a Jasco V-570 UV–Vis spectrophotometer equipped with NV-470 type integrating sphere. A BaSO_4 disk was used as reference. All spectra were recorded under ambient conditions.

The reducibility of the modified samples was investigated by temperature programmed reduction (TPR) technique in H_2/Ar flow (10:90, 20 mL/min) using a conventional TPR apparatus equipped with a heat conductivity cell and a trap for removal of released water. The reducibility of the metal oxide species was estimated by measuring the hydrogen uptake of the samples.

Mössbauer spectra were collected at 300 K and 77 K in constant acceleration mode after successive in situ thermal treatments in vacuum (10^{-1} Pa) at 640 K or reduction in hydrogen at the same temperature for 90 min. In the least-squares fitting process Lorentzian line shape was assumed and positional parameters were not constrained. Isomer shift data were related to the center of the α -iron spectrum. The accuracy of positional data was estimated to be ± 0.03 mm/s. Coordination assignments are based on characteristics reported by Burns [36], i.e., for Fe(III) increasing symmetry results in a decrease, but an increase of quadrupole splitting in the spectra of Fe(II) . For some typical spectral components these assignments are indicated in Table 2.

FT-IR experiments were performed with a Nicolet Compact 6700 spectrometer by self-supported wafer technique, using pyridine (Py) (0.07 kPa) as probe molecule. The spectra were normalized to 5 mg/cm^2 weight of wafers for comparison.

The EPR spectra were recorded on a BRUKER ER 200D SRC spectrometer operating in X-band. Standard (ER4102) rectangular (TE_{102} mode) EPR cavity was used. The modulation of the magnetic field was 100 kHz. The samples were accommodated in quartz sample tubes with i.d. 4 and o.d. 5 mm. The *g*-factors were determined relative to the “EPR marker” available in the FF-Lock module (ER031) with an accuracy of ± 0.0001 . It was calibrated by using DPPH as a reference standard ($g = 2.0036$) [37].

2.3 Catalytic Activity Measurements

Prior to the catalytic test the samples were pretreated in hydrogen up to 723 K for 1.5 h. Cyclohexanol dehydrogenation was studied at atmospheric pressure using a fixed-bed flow reactor, nitrogen as carrier gas and 30 mg sample (particle size 0.2–0.8 mm) diluted with 60 mg glass beads of the same diameter previously checked to be inactive. The nitrogen stream passed through a saturator filled with cyclohexanol and equilibrated at 342 K ($n_{\text{N}_2}/n_{\text{cyclohexanol}} = 38$). The activity was determined at 513 and 533 K. On-line analysis of the reaction products was performed using HP-GC with a 25 m HP-35 capillary column.

3 Results and Discussion

3.1 Physico-Chemical Characterization of the Samples

Small angle XRD patterns (Fig. 1) of the parent silica material exhibit reflections typical of hexagonally arranged pore structure. XRD data of the modified samples in this region confirm the preservation of the hexagonal structure after the modification process. The shift of the position of the (100) reflection is more distinguished for bicomponent materials in comparison with the parent and the mono-component ones, which could be assigned to the higher degree of the incorporation of the metal ions in the silica framework (Table 1). Partial silica matrix collapse can be assumed only for FeTiMCM-41(1), where significant intensity decrease of (100) reflection confirms the lower long range ordering of the structure. In the wide-angles region no characteristic reflections of any iron and/or titanium containing species are registered, suggesting their predominant incorporation into the MCM-41 silica framework.

In Fig. 2 nitrogen physisorption isotherms of the FeTiMCM-41 materials are presented. The corresponding calculated parameters are listed in Table 1. The isotherms of FeTiMCM-41 materials are of type IV (IUPAC classification), with a capillary condensation step at about 0.25 p/p_0 , characteristic for mesoporous materials. High metal loading (FeTiMCM-41(1)) results in some deterioration of the structure characterized by somewhat lower specific surface area, however, the pore diameter does not decrease. All the catalysts exhibit H3–H4 type of hysteresis loop, which can be associated with the formation of slit-like secondary mesopores or defect sites. This secondary mesoporosity is an indication of some structural disorder, however, can enhance the mass transfer properties of the mesoporous material. The BET surface area and the pore

volume of all the modified materials slightly decreased in comparison with the parent MCM-41 (Table 1). The increase in the pore size can be predominantly due to the metal incorporation into the silica matrix [35].

The UV–Vis spectra (Fig. 3) of the modified materials exhibit a broad absorption peak in the 220–250 nm region attributable to isolated, tetrahedrally coordinated metal species [6, 7, 38, 39]. The band at about 350 nm, characteristic for all iron containing samples most probably arise from the presence of oligomeric FeO_x species in the silica matrix. The intensity of this band is higher for samples with higher amount of iron and low amount of titanium (FeTiMCM-41(3)). The low intensity band at about 500 nm in the spectra of bicomponent materials with high iron content indicate the presence of either extra-framework iron and/or iron oxide particles [6, 39]. According to [39], this peak can be assigned to symmetrical and spin forbidden d–d transitions of Fe^{3+} , meaning that iron oligomers (low nuclearity $2d\text{-FeO}_x$ species or ferric species ($3d\text{-Fe}_2\text{O}_3$)) are formed.

Mössbauer spectroscopy is applied for more detailed characterization of the iron species [5, 40–42]. The spectra of all studied materials after different pretreatments are presented in Fig. 4 and Table 2. Only Fe^{3+} doublets can be detected in hydrated, template free samples. Fe^{3+} can be found in coordinations with different symmetries. Species with lower QS value correspond to octahedral coordination with higher symmetry, whereas those with higher QS value to distorted octahedral surroundings. According to our former investigations [42, 43] these octahedral species can be interpreted as Fe^{3+} atoms trigonally and tetrahedrally incorporated into the silica framework through oxygen atoms and surrounded by silanol groups and/or coordinating water molecules. Removal of the adsorbed water molecules results in the appearance of distorted tetrahedrally coordinated Fe^{3+} species similar to

Fig. 1 XRD patterns of the studied samples

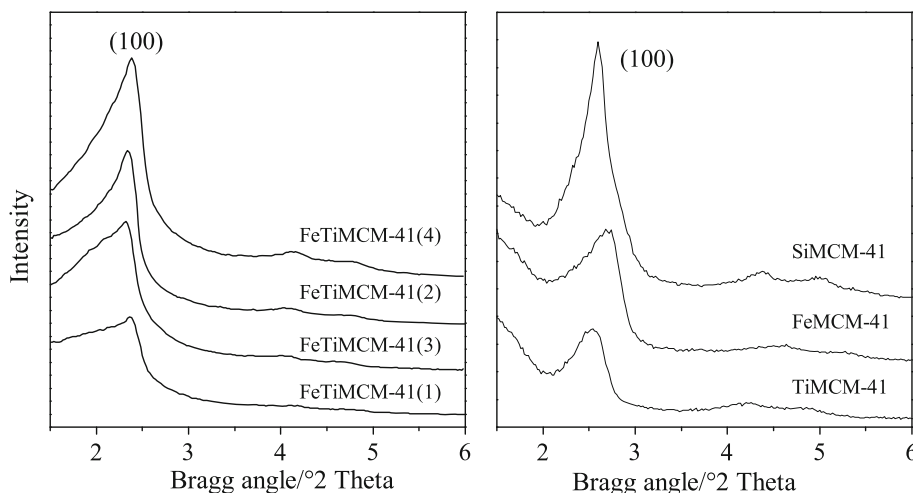
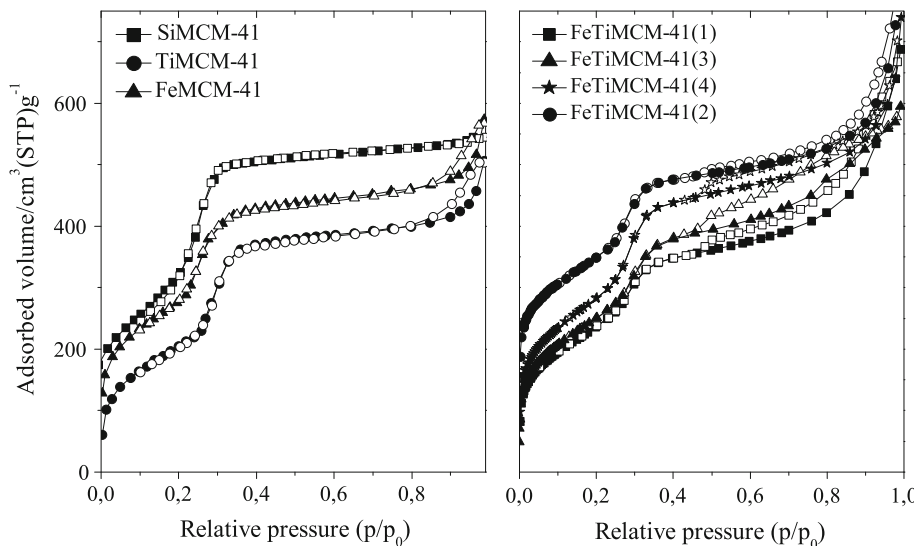
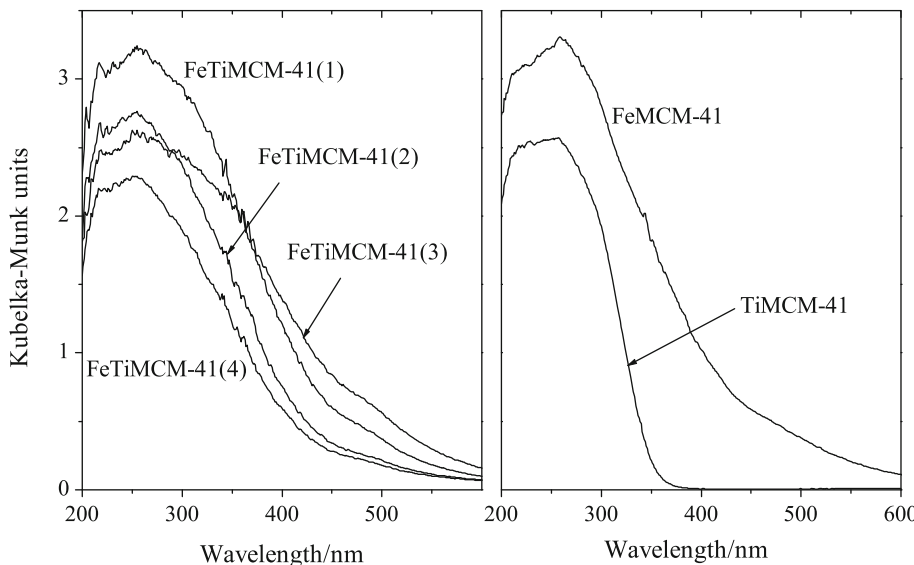


Table 1 Physico-chemical properties of the studied samples

Samples	Si/Ti	Si + Ti/Fe	Fe cont. (%)	Ti cont. (%)	S_{BET} (m^2/g)	PD ^a (nm)	Pore vol. ^a (cm^3/g)	a_0 ^b (nm)
SiMCM-41	—	—	—	—	1198	2.3	1.00	3.94
TiMCM-41	10	—	—	6.68	907	2.6	0.90	4.06
FeMCM-41	—	20	4.35	—	984	2.3	0.90	3.95
FeTiMCM-41(1)	10	15	5.54	6.47	812	2.5	0.99	4.31
FeTiMCM-41(2)	10	25	3.42	6.68	845	2.4	0.97	4.35
FeTiMCM-41(3)	20	15	5.61	3.43	845	2.5	0.88	4.40
FeTiMCM-41(4)	20	25	3.48	3.55	973	2.5	0.99	4.28

^a Pore diameter and pore volume calculated by the BJH method (desorption branch)^b Cell parameter ($a_0 = 2d_{100}(3)^{-1/2}$)**Fig. 2** Nitrogen adsorption/desorption isotherms of the titanium and iron modified mesoporous materials (the curves are shifted in y-direction in order to prevent overlapping)**Fig. 3** UV–Vis spectra of the mono- and bicomponent materials

mono-component FeMCM-41 (IS = 0.32, QS = 1.47). Formation of Fe^{2+} after the evacuation is due to autoreduction of Fe^{3+} in framework position. The reduction even

at 640 K resulted in almost total reduction to Fe^{2+} , only a small fraction (5–17%) of iron remained in trivalent state. Fe^{2+} species can be found also in different coordination

Fig. 4 Mössbauer spectra of the studied samples after different pretreatments

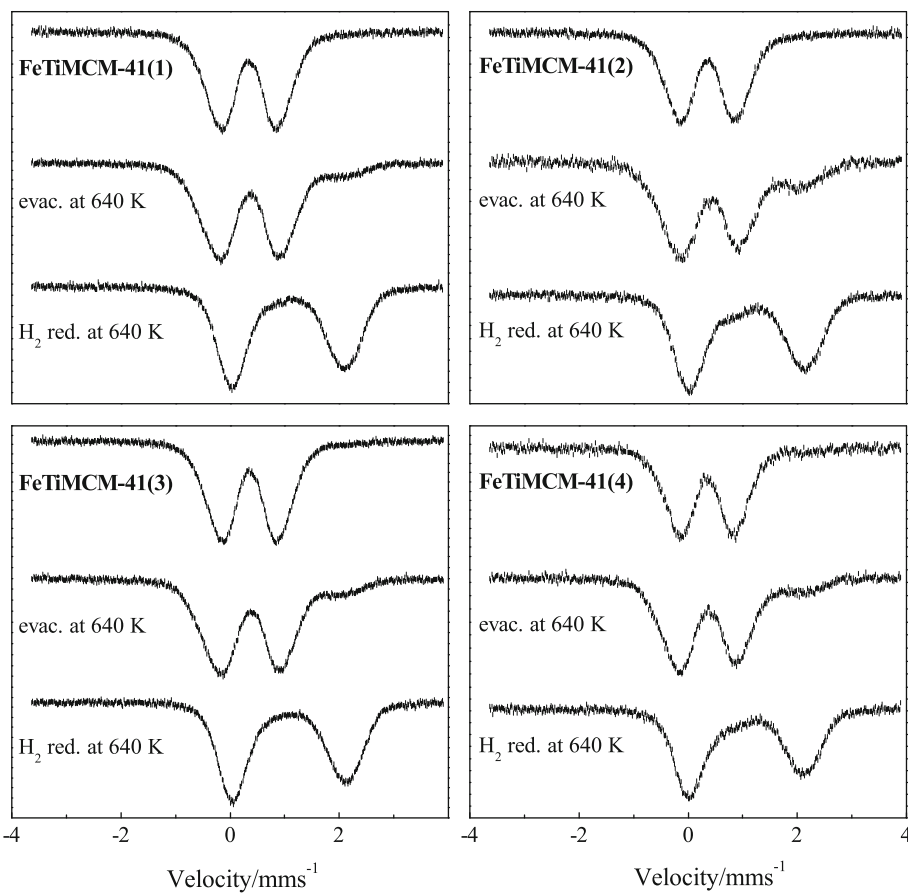


Table 2 Mössbauer data of FeTiMCM-41 samples

Samples	Comp.	FeTiMCM-41(1)			FeTiMCM-41(2)			FeTiMCM-41(3)			FeTiMCM-41(4)		
		IS	QS	RI									
Parent	Fe ³⁺	0.33	0.81	60	0.33	0.79	38	0.34	0.81	43	0.34	0.77	38
	Fe ³⁺	0.33	1.30	40	0.34	1.26	62	0.33	1.30	57	0.33	1.22	62
Evacuation at 640 K	Fe ³⁺	0.35	0.90	40	0.39	0.88	43	0.35	0.87	33	0.35	0.88	45
	Fe ³⁺	0.32	1.47	50	0.35	1.47	32	0.32	1.42	53	0.32	1.43	40
Reduction in H ₂ at 640 K	Fe ²⁺	1.00	2.33	10	0.90	2.34	25	0.98	2.26	13	1.00	2.32	15
	Fe ³⁺	0.32	0.44	5	0.42	0.69	12	0.24	0.25	4	0.41	0.42	17
	Fe ²⁺	1.03	1.82	57	1.03	1.88	56	1.03	1.84	60	0.91	2.06	42
	Fe ²⁺	1.07	2.36	38	1.07	2.46	32	1.08	2.36	35	1.17	2.18	41

states, either in tetrahedral or in octahedral. According to Mössbauer spectroscopic investigations our catalysts with different amounts of metal behave similar. One exception is that FeTiMCM-41(1) has 20% higher amount of highly symmetrical octahedrally coordinated Fe³⁺ than the other catalysts. There is also significant difference between the extents of auto-reduction of the samples, having FeTiMCM-41(2) the highest value (25%). Auto-reduction can be associated with the release of oxygen from the framework, which means that iron is connected to the silica–titania

framework with weaker bonds and formation of Fe–O–Fe chains can be assumed [43].

The TPR profiles of the iron-containing materials (not shown) exhibit a well pronounced TPR peak between 500 and 870 K with a maximum at about 700 K. The calculated hydrogen uptake (Table 3) for FeMCM-41 corresponds to one electron transfer, i.e., Fe³⁺ incorporated into the silica matrix could be reduced only to Fe²⁺ state up to 870 K [34, 41]. The calculated extent of reduction of FeTiMCM-41(1) and FeTiMCM-41(3) catalysts is slightly over 100%,

Table 3 TPR data of iron and titanium modified MCM-41 samples

Samples	Fe content ^a (mmol/g _{calc})	Ti content ^a (mmol/g _{calc})	H ₂ uptake ^b (mmol/g _{calc})	Extent of reduction ^c (%)
TiMCM-41	–	1.47	0.058	7.9
FeMCM-41	0.78	–	0.39	100
FeTiMCM-41(1)	0.99	1.39	0.55	109
FeTiMCM-41(2)	0.62	1.39	0.28	92
FeTiMCM-41(3)	1.01	0.70	0.51	102
FeTiMCM-41(4)	0.62	0.70	0.29	95

^a Related to 1 g sample calcined at 1273 K

^b Calculated from the area of the TPR curve in the range of 373–1073 K

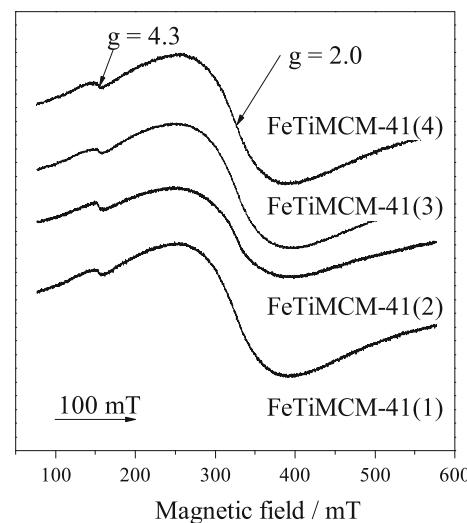
^c Calculated from the H₂ uptake related to the total amount of iron for all iron-containing samples and titanium for TiMCM-41, assuming that 0.5 mmol H₂ is needed for the reduction of 1 mmol Fe³⁺ to Fe²⁺ and for that of 1 mmol Ti⁴⁺ to Ti³⁺

which can be explained by the reduction of some “extra framework” iron species to metallic state. However, the magnetic sextet typical of large Fe–O–Fe clusters did not appear in the Mössbauer spectrum of the samples. The lower hydrogen uptake of bicomponent materials with lower iron and higher titanium loading in comparison to FeMCM-41 and the bicomponent materials with higher iron and lower titanium contents could be assigned to the more difficult reduction of the iron species of the former materials (Table 3). Changes of the iron environment, probably due to the formation of Ti–O–Fe-type species can be responsible for this decreased reducibility. These results are in good accordance with the Mössbauer data where higher amount of Fe³⁺ is registered for FeTiMCM-41(2) and FeTiMCM-41(4) samples after reduction (Table 2). The reduction ability of TiMCM-41 is significantly lower (approx. 8% up to 1023 K) [34, 35] in comparison to all iron-containing samples.

EPR spectra of the bicomponent FeTiMCM-41 samples are presented in Fig. 5. The spectra consist of (i) a signal at about 160 mT ($g = 4.3$) and (ii) a broad, rather featureless signal centered at about 320 mT ($g = 2.0$). These two signals are typical of Fe(III) within or on the surface of a siliceous material. The signal at $g = 4.3$ is due to isolated Fe(III) ions in a distorted tetrahedral coordination while the EPR signal at $g = 2.0$ clearly indicates tetrahedrally coordinated Fe³⁺ species [44–47]. The broad spectral component is due to the presence of oligomeric iron oxide species. The absence of signal at $g = 2.2$ in all the bicomponent samples suggests the absence of non-framework (superparamagnetic) iron oxide nanoparticles dispersed in the mesoporous channels [47]. The detected iron species in tetrahedral coordination for bicomponent samples are in good accordance with their XRD, TPR, UV–Vis and Mössbauer spectroscopic data.

FT-IR spectra of adsorbed Py on the selected samples after evacuation at 623 K are presented in Fig. 6. The samples exhibit typical band pairs of Lewis and Brönsted

acid sites [13, 48]. In TiMCM-41 sample the 1447/1608 cm⁻¹ band pair can be associated with Lewis acidic Ti–O–Si sites in the MCM-41 structure, whereas at 1544/1638 cm⁻¹ the weak bands of protonated pyridinium ion appear, evidencing the presence of Brönsted acidic Ti–O–Si bridges, where Ti atoms are in pentahedral/octahedral coordination surrounded by hydroxyl groups or water molecules [13]. In FeMCM-41 catalyst the Lewis and Brönsted acidic bands appear at higher wavenumbers, at 1452/1612 cm⁻¹ and at 1548/1638 cm⁻¹, respectively. In the FT-IR spectra of FeTiMCM-41(1) and FeTiMCM-41(3) samples the presence of Lewis and Brönsted acid sites belonging to both titanium and iron species can be observed at 1447/1452 cm⁻¹ and at 1548 cm⁻¹, respectively. Upon reduction at 723 K in H₂ the weak 1454 cm⁻¹ band, characteristic for Brönsted acidic sites disappear for all the catalysts (not shown). However, the increase of Lewis acidic sites can only be observed for the FeTiMCM-41(1) sample.

**Fig. 5** EPR spectra of the TiFeMCM-41 samples

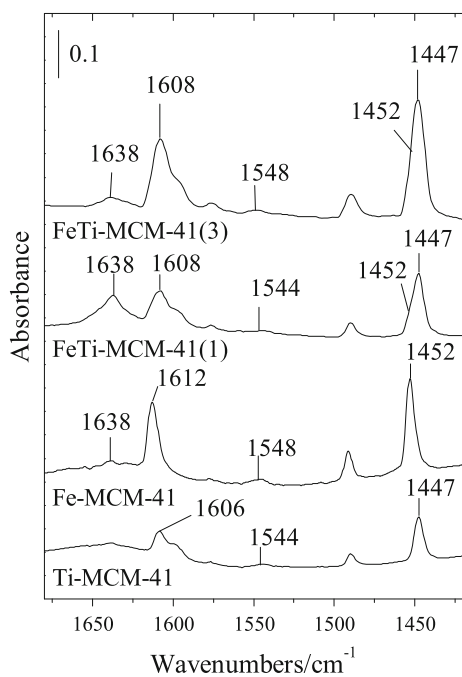


Fig. 6 FT-IR spectra of adsorbed Py on the mono and bicomponent samples. Before Py adsorption at 373 K, the samples were evacuated at 623 K. Py was desorbed at 473 K

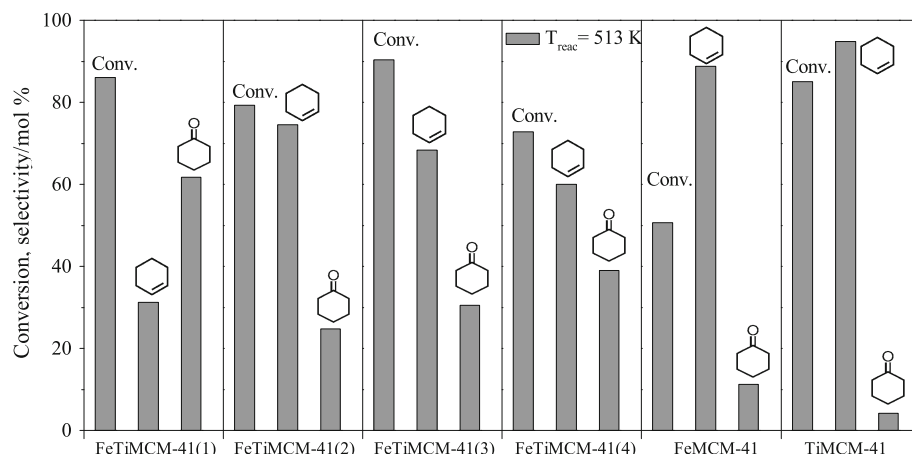
3.2 Catalytic Activity for Cyclohexanol Dehydrogenation

In Fig. 7 the catalytic activities of mono- and bicomponent iron and/or titania containing MCM-41 materials in cyclohexanol dehydrogenation at 513 K are presented. Catalysts were pretreated in hydrogen at 723 K before catalytic reaction. Monocomponent FeMCM-41 shows lower activity but somewhat higher selectivity to cyclohexanone at 513 K in comparison to monocomponent TiMCM-41. Evidenced also by our FT-IR investigations, in titania containing catalyst Ti–O–Si bridges may generate Brønsted acid sites, if the Ti atoms are in pentahedral/

octahedral coordination and hydroxyl groups or water molecules can be found in their coordination sphere [13]. Our previous study showed [35] that only a small part (about 8%) of Ti^{4+} species can be reduced to Ti^{3+} in this type of silica, consequently reduction does not change the structure of TiMCM-41 significantly. However, the amount of Brønsted acid sites ($\text{Si}-\text{O}_3 \equiv \text{Fe}(\text{OH})-\text{Si}$) in FeMCM-41, responsible for the formation of cyclohexene is decreased by the reduction of Fe^{3+} to Fe^{2+} . Fe^{2+} can act as a Lewis acid site enhancing the production of cyclohexanone. Catalytic data of monocomponent samples suggest that the reaction pathway is dominated by Brønsted acid sites. Activity loss of FeMCM-41 can be explained by the lower stability against reaction product water compared to the titania containing varieties. A part of iron is probably transformed to FeO_x oligomers, not active in cyclohexanol dehydrogenation. TiMCM-41 catalyst has the highest catalytic activity and selectivity to cyclohexene.

All bicomponent samples show higher selectivity to cyclohexanone in comparison to the monocomponent ones. FeTiMCM-41(1) and FeTiMCM-41(3) catalysts show the highest catalytic activity and the former one also high selectivity to cyclohexanone (60%). FeTiMCM-41(1) sample contains the highest amount of iron and titania. Textural characteristics show that incorporation of such high amount of metals hinders the formation of well ordered MCM-41 materials and increase the reducibility. Our Py adsorption FT-IR investigations (not shown) confirmed the increasing amount of Lewis acid sites in this sample upon reduction. However, formation of $\text{Ti}-\text{O}-\text{Fe}$ bonds can also be assumed, where electron transfer from $\text{Ti}-\text{O}$ to $\text{Fe}-\text{O}$ enhance the strength of $\text{Fe}-\text{O}$. The reduction of Fe^{3+} results in the formation oxygen vacancy site involving a two-coordinated divalent Fe and one site in which the reduced iron remains in the trigonal coordination state. Trigonally coordinated Fe^{2+} sites act as strong Lewis acid sites. According to the literature the Lewis acid–base pairs react with an alcohol molecule to generate an

Fig. 7 Catalytic activity and selectivity at 513 K of the TiFeMCM-41 samples after reduction in H_2 at 723 K



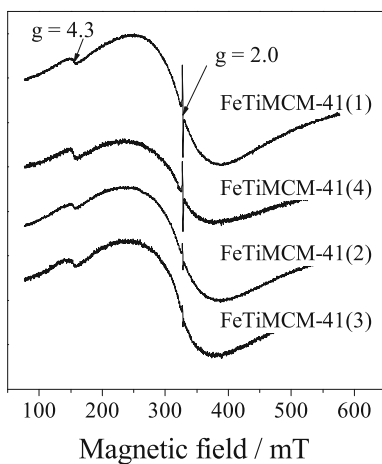
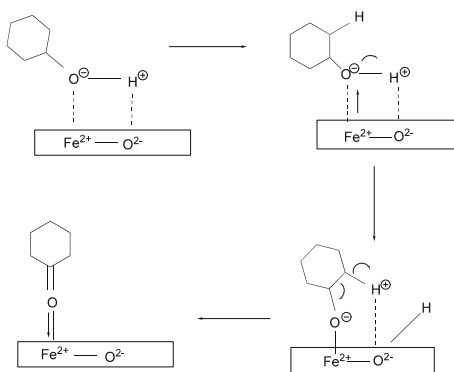


Fig. 8 EPR spectra of the spent catalysts



Scheme 1 Mechanism of cyclohexanol dehydrogenation

adsorbed long-lived alkoxy intermediate [24]. The EPR spectra of the spent catalysts (Fig. 8) show the presence of a singlet at $g = 2.0$ due to the formation of oxygen species. The intensity of this signal is higher for FeTiMCM-41(1) and FeTiMCM-41(4), possessing the higher selectivity to cyclohexanone. During the catalytic process the adsorbed oxygen species have an important role [24]. The surface oxygen species act as Lewis bases which extract hydrogen from cyclohexanol and from the intermediates (Scheme 1). At the same time, iron species act as Lewis acid sites to stabilize the adsorbed negatively charged intermediates.

4 Conclusion

Mono- and bicomponent, iron and titanium containing MCM-41 materials were synthesized by sol-gel method. Formation of Fe^{3+} and Ti^{4+} ions incorporated into the silica structure, located in tetrahedral and octahedral positions was registered for all studied materials. All metal modified materials showed high catalytic activity in cyclohexanol conversion. After reduction in hydrogen at

723 K formation of stabilized Fe^{2+} species and increased selectivity to cyclohexanone was observed on FeTiMCM-41 materials. The highest catalytic activity and selectivity to cyclohexanone could be obtained for the FeTiMCM-41 sample with the highest metal content ($\text{Si/Ti} = 10$ and $\text{Si} + \text{Ti/Fe} = 15$), where increased Lewis acidity was evidenced and formation of $\text{Ti}^{4+}/\text{Fe}^{2+}$ ion pairs was assumed.

Acknowledgments Financial support by the project DO02-295_2008 and the Bulgarian-Hungarian Inter-academic Exchange Agreement are greatly acknowledged.

References

1. Corma A (1997) *Chem Rev* 97:2373
2. Wang Y, Zhang Q, Shishido T, Takehira K (2002) *J Catal* 209:186
3. Wu Ch, Kong Y, Gao F, Wu Y, Lu Y, Wang J, Dong L (2008) *Microporous Mesoporous Mater* 113:163
4. Garvalho WA, Varaldo PB, Wallau M, Schuchardt U (1997) *Zeolites* 18:408
5. Kawabata T, Ohishi Y, Itsuki S, Fujisaki N, Shishido T, Takaki K, Zhang Q, Wang Y, Takehira K (2005) *J Mol Catal A* 236:99
6. Hamdy MS, Mul G, Jansen JC, Ebaid A, Shan Z, Overweg AR, Maschmeyer Th (2005) *Catal Today* 100:255
7. Orlov A, Zhal Q-Z, Klinowski J (2006) *J Mater Sci* 41:2187
8. Araujo RS, Azevedo DCS, Rodriguez-Castellon E, Jimenez-Lopez A, Cavalcante CL Jr (2008) *J Mol Catal A* 281:154
9. Taguchi A, Schüth F (2005) *Microporous Mesoporous Mater* 77:1
10. Rodriguiz ACC (2007) *Catal Commun* 8:1227
11. Sobczak I, Ziolek M, Renn M, Decyk P, Nowak I, Daturi M, Lavallee J-C (2004) *Microporous Mesoporous Mater* 74:23
12. Szegedi A, Hegedüs M, Margitfalvi JL, Kiricsi I (2005) *Chem Commun* 11:1441
13. Kataoka T, Dumesic JA (1988) *J Catal* 112:66
14. Kang M, Lee M-H (2005) *Appl Catal A* 284:215
15. Zhou M, Yu J, Chang B (2006) *J Hazard Mater B* 137:1838
16. Lihitkar NB, Abyaneh MK, Samuel V, Pasricha R, Gosavi SW, Kulkarni SK (2007) *J Colloid Interface Sci* 314:310
17. Galacho C, Carrott MMLR, Carrot PJM (2007) *Microporous Mesoporous Mater* 100:312
18. Ji D, Zhu W, Wang Zh, Wang G (2007) *Catal Commun* 8:1891
19. Reddy BM, Ratnam KJ, Saikia P (2006) *J Mol Catal A* 252:238
20. Elangovan SP, Murugesan V (1997) *J Mol Catal A* 118:301
21. Fridman VZ, Davydov AA (2000) *J Catal* 195:20
22. Fridman VZ, Davydov AA, Titievsky K (2004) *J Catal* 222:545
23. Park C, Keane MA (2001) *J Mol Catal A* 166:303
24. Yang Zh, Li J, Yang X, Xie X, Wu Y (2005) *J Mol Catal A* 241:15
25. Mishra BG, Rao GR (2006) *J Mol Catal A* 243:204
26. Reddy GK, Rao PK (1997) *Catal Lett* 45:93
27. Nagaraja BM, Kumar VS, Shashikala V, Padmasri AH, Reddy SS, Raju BD, Rao KSR (2004) *J Mol Catal A* 223:339
28. Carlos DV, Perez CA, Salim VMM, Schmal M (1999) *Appl Catal A* 176:205
29. Mendes FMT, Schmal M (1997) *Appl Catal A* 163:153
30. Bautista FM, Campelo JM, Garcia A, Luna D, Martinas JM, Quiros RA, Romero AA (2003) *Appl Catal A* 243:93
31. Reddy GK, Rao KSR, Rao PK (1999) *Catal Lett* 59:157
32. Chen W-Sh, Lee M-D, Lee J-F (1992) *Appl Catal A* 83:201

33. Dobrovolszky M, Tétényi P, Paál Z (1982) *J Catal* 74:31
34. Popova M, Szegedi A, Cherkezova-Zheleva Z, Mitov I, Kostova N, Tsoncheva T (2009) *J Hazard Mater* 168:226
35. Popova M, Szegedi A, Kostova N, Tsoncheva T (2008) *Catal Commun* 10:304
36. Burns RG (1994) *Hyperfine Interact* 91:739
37. Yordanov ND, Lubenova S (2000) *Anal Chim Acta* 403:305
38. Ahn W-S, Kim N-K, Jeong S-Y (2001) *Catal Today* 68:83
39. Chmielarz L, Kustrowski P, Drozdek M, Dziembaj R, Cool P, Vansant EF (2006) *Catal Today* 114:319
40. Kim DH, Woo SI, Moon SH, Kim HD, Kim BY, Cho JH, Joh YG, Kim EC (2005) *Solid State Commun* 136:554
41. Dzwigaj S, Stievano L, Wagner FE, Che M (2007) *J Phys Chem Solids* 68:1885
42. Lazar K, Fejes P, Pal-Borbely G, Beyer HK (2002) *Hyperfine Interact* 141/142:387
43. Szegedi A, Pál-Borbély G, Lázár K (2001) *React Kinet Catal Lett* 74:277
44. Vinu A, Nandhini KU, Murugesan V, Bohlmann W, Umamaheswari V, Poppl A, Hartmann M (2004) *Appl Catal A* 265:1
45. Bourlinos AB, Karakassides MA, Petradis D (2000) *J Phys Chem B* 104:4375
46. Goldfarb D, Strohmaier KG, Vaughan DEW, Thomann H, Poluektov OG, Schmidt J (1996) *J Am Chem Soc* 118:4665
47. Xin H, Liu J, Fan F, Feng Zh, Jia G, Yang Q, Li C (2008) *Microporous Mesoporous Mater* 113:231
48. Szegedi A, Kónya Y, Méhn D, Solymár E, Pal-Borbély G, Horváth Y, Biró L, Kiricsi I (2004) *Appl Catal A* 272:257